

Spitzer observations of the Orion OB1 association: second generation dust disks at 5-10 Myr

Jesús Hernández^{1,2}, César Briceño², Nuria Calvet¹, Lee Hartmann¹, James Muzerolle³ and Amilkar Quintero^{4,5}

jesush@cida.ve

ABSTRACT

We report new Spitzer observations of intermediate mass stars in two regions of the Orion OB1 association located in the subassociations OB1a (\sim 10 Myr) and OB1b (\sim 5 Myr). In a representative sample of stars earlier than F5 of both stellar groups, we find a population of stars surrounded of debris disks, without excess in the IRAC bands and without emission lines in their optical spectra, but with a varying degree of $24\mu\text{m}$ excess. Comparing our samples with $24\mu\text{m}$ observations of intermediate mass stars in other stellar groups, spanning a range of ages from 2.5 Myr to 150 Myr, we find that debris disks are more frequent and have larger $24\mu\text{m}$ excess at 10 Myr (OB1a). This trend agrees with predictions of models of evolution of solids in the outer regions of disks (>30 AU), where large icy objects (\sim 1000 Km) begin to form at \sim 10 Myr; the presence of these objects in the disk initiates a collisional cascade, producing enough dust particles to explain the relatively large $24\mu\text{m}$ excess observed in OB1a. The dust luminosity observed in the stellar groups older than 10 Myr declines roughly as predicted by collisional cascade models. Combining Spitzer observations, optical spectra and 2MASS data, we found a new Herbig Ae/Be star (HD290543) and a star (HD36444) with a large $24\mu\text{m}$ excess, both in OB1b. This last object could be explained as a intermediate stage between HAeBe and true debris systems or as a massive debris disk produced by a collision between two large objects (>1000 Km).

¹Department of Astronomy, University of Michigan, 830 Dennison Building, 500 Church Street, Ann Arbor, MI 48109, US

²Centro de Investigaciones de Astronomía, Apdo. Postal 264, Mérida 5101-A, Venezuela.

³Steward Observatory, University of Arizona, 933 North Cherry Avenue, Tucson, AZ 85721, US

⁴Universidad de Carabobo, FACYT, Dept. de Física, Venezuela

⁵Visiting student at CIDA

Subject headings: infrared: stars: formation — stars: pre-main sequence — open cluster and associations: individual (Orion OB1) — protoplanetary systems: protoplanetary disk

1. Introduction

Theories of star formation indicate that, in general, stars are born surrounded by disks due to angular momentum conservation (Hartmann 2005). These optically thick primordial disks, which contain gas and dust, are expected to evolve by accreting gas into the star and planets, while dust grains grow and settle towards the mid-plane of the disk. As the primordial disk evolves from optically thick to optically thin, its excess at near and mid infrared wavelength diminishes drastically. The time scale for this evolution is strongly dependent on the stellar mass (Lada & Lada 1995; Muzerolle et al. 2003; Calvet et al. 2004; Sicilia-Aguilar et al. 2005); in particular, for low mass stars (K5 or later), $\sim 90\%$ of the stars have lost their primordial disk at about 5-7 Myr (Haisch et al. 2001; Hillenbrand et al. 2005), while for objects in the mass range of the Herbig Ae/Be (HAeBe) stars ($\sim 2-8M_{\odot}$), the time scale for primordial disk dissipation is less than ~ 3 Myr (Hernández et al. 2005). Theories of dust evolution in the solar nebula indicate that the timescale for disk evolution is also proportional to the orbital period (Weidenschilling 1997; Dullemond & Dominik 2004); so, grain growth and settling to the mid-plane occur fastest in the inner disk resulting in a faster decline of disk emission at shorter wavelength (Hartmann 2005; Sicilia-Aguilar et al. 2006; Lada et al. 2006). In this "clearing phase", stars could evolve to "transition disk objects" in which we find an inner optically thin region with an outer optically thick primordial disk (Calvet et al. 2002; D'Alessio et al. 2005; Calvet et al. 2005). Since a small fraction of transition objects are observed in several star formation regions (e.g., Sicilia-Aguilar et al. 2006; Muzerolle, et al 2006), this phase has to be very brief (Kenyon & Bromley 2004a). After this brief phase, second generation dusty disks (debris disks) are frequently observed at mid and far IR wavelength in stars with age from few Myr to several Gyr (e.g., Rieke et al. 2004; Decin et al. 2003; Bryden et al. 2006; Chen et al. 2005a,b). Since radiation pressure, Poynting-Robertson drag, ice sublimation and other processes remove the dust on short timescales compared with the age of the system, the observed dust must have been replenished from a reservoir, such as sublimation of comets or collisions between parent bodies (e.g., Chen et al. 2006; Kenyon & Bromley 2004b; Dominik & Decin 2003). In the collisions scenario, models of debris disk evolution suggest that the formation of disks coincides with the formation of large icy objects (1000 Km) at 10-30 Myr, which stir up the leftover objects in the disks originating a collisional cascade that produces a copious amount of dust observed in young debris disk stars (Kenyon & Bromley 2005, 2004a,b; Decin et al.

2003). For A-type stars, Kenyon & Bromley (2002, 2004b) and Dominik & Decin (2003) show that, as the debris reservoir diminishes and the dust is removed, the luminosities of the debris disks decay in several hundred millions years, following a simple exponential law, age^{-1} . Observations confirm this long period trend (Decin et al. 2003; Rieke et al. 2005). HAeBe stars are the precursors of A-type stars with debris disks, like Vega or β Pic. However, details of the earlier processes by which the primordial disk evolves to transition disk and to debris disk are not well understood.

In this contribution, we address the questions of disk dissipation and debris disk formation in the mass range of HAeBe. We present Spitzer space telescope data for intermediate mass stars located in two regions with different evolutionary stages in the Orion OB1 association, one of the largest and nearest regions with active star formation. The selection of the samples and observations are described in §2. We analyze the observations and describe the results on §3 and give our conclusions in §4.

2. Observations and sample selection

We have obtained near-infrared (NIR) and mid-infrared photometry of two regions in the Orion OB1 association using the 24 μm band of the Multiband Imaging Spectrometer for Spitzer (MIPS; Rieke et al. 2004) and the four channels (3.6, 4.5, 5.8 & 8.0 μm) of the InfraRed Array Camera (IRAC, Fazio et al. 2004), instruments on board the Spitzer Space Telescope. Figure 1 shows the positions of the MIPS (thick solid line) and IRAC¹ (thin solid line) fields in the Orion OB1 association. One of these fields is located on the Orion OB1a sub-association with an age of 10 Myr (Briceño et al. 2006) and the other field is located on the Orion OB1b sub-association with an age of 5 Myr (Briceño et al. 2005). Using isocontours of the dust infrared emission map (Schlegel et al. 1998) we can estimate that at least 90% of the area in OB1a has visual extinctions smaller than $A_V \sim 0.12$ and at least 90% of the area in OB1b has visual extinctions smaller than $A_V \sim 0.6$. Table 1 includes more information about the MIPS fields and the related stellar groups.

MIPS observations were done using medium scan mode with full-array cross-scan overlap, resulting in a total effective exposure time per pointing of 40 seconds. The images were processed using the MIPS instrument team Data Analysis Tool (DAT), which calibrates the data and applies a distortion correction to each individual exposure before combining into a final mosaic (Gordon et al. 2005). We also applied an additional correction to remove a faint readout-dependent residual pattern. We obtained point source photometry at 24 μm

¹Figure 1 shows the IRAC bands 1 and 3, the bands 2 and 4 have a 8' displacement to the north

with IRAF/daophot point spread function fitting, using an aperture size of about 5.7" and an aperture correction factor of 1.73 derived from the STinyTim PSF model. The absolute flux calibration uncertainty is less than 5%. Our final flux measurements are complete down to about 1 mJy in both maps.

The IRAC observations were done using a standard raster map with 290" offsets, to provide maximum areal coverage with just a slight overlap between frames, to aid in mosaicking the data. Each position is composed of 3 dithers. The single-frame integration was 12 seconds. The IRAC Basic Calibrated Data (BCD) were processed using the *IRACproc* (Schuster et al. 2006) package. *IRACproc* improves cosmic ray and other transient rejection by using spatial derivative images to map the locations and structure of astronomical sources. Because the native IRAC images are under/critically sampled (1.22 arcsec/pixel), the PSF is subject to large variations in shape between successive frames because of sub-pixel shifts caused by dithering or telescope jitter. The software is designed to preserve the photometric integrity of the data, especially of bright sources, by applying a metric that accounts for these large variations in the PSF. Although *IRACproc* was originally developed for the Nearby Stars Guaranteed Time Observer (GTO) program, which was based on a 5-point small scale dither pattern, our IRAC 3-point dither observations were sufficient to provide a reliable cosmic ray/transient rejection. The final mosaics created with *IRACproc* have a scale of 0.86 arcsec/pixel. We extracted the photometry using the *apphot* package in IRAF, with an aperture radius of 12 arcsec and a background annulus from 12 to 22.4 arcsec. Because IRAC standard stars were measured with the same aperture and sky annulus, we did not apply an aperture correction. We adopted zero-point values of 19.660, 18.944, 16.880, 17.394 in the [3.6], [4.5], [5.8] and [8] bands, respectively (Hartmann 2005). Since MIPS and IRAC fields do not cover the same area on the sky (see Figure 1), some objects were not observed in all IRAC channels. However, the results shown in §3 are based mainly on the MIPS data.

To find the early type stars (F5 or earlier) in both fields, we selected from the 2MASS catalog (Cutri et al. 2003) stars with $J < 10.3$ for the OB1a field and $J < 11.0$ for the OB1b field. These limits were calculated using the V magnitude (Cox 2000) and the V-J color (Kenyon & Hartmann 1995) for a main sequence star with spectral type F5, and the distances and the visual extinctions in Table 1. Using the Cardelli et al. (1989) extinction law with $R_V = 3.1$, we transformed visual extinctions to reddening in the NIR bands. The NIR color color diagrams, $[J-H]$ versus $[H-K]$ (upper panels of Figure 2), for the stars selected in both fields reveal that most of the stars are located on the main sequence locus (Bessell & Brett 1988). Therefore, these stars have little extinction and small or no NIR excesses. Only two objects, V346 Ori in OB1a and HD290543 in OB1b, appear in the HAeBe stars loci (Hernández et al. 2005), where the NIR excess can be explained by emission from an optically thick primordial disk with a sharp dust-gas transition at the dust destruction radius (e.g., Dullemond & Dominik

2004; Muzerolle, et al 2004). V346 Ori and HD290543 are included as members of OB1a and OB1b, respectively. The dotted horizontal lines in the upper panels of Figure 2 are the [J-H] limits corresponding to a F5 star with $A_V=0.12$ for OB1a and to a F5 star with $A_V=0.6$ for OB1b. The lower panels of Figure 2 show the color-magnitude diagrams, [J-H] versus J, for the stars below the [J-H] limits in the upper panels and the stars with thick primordial disk (solid triangles). The solid lines represent the Zero Age Main Sequence (ZAMS) from Palla & Stahler (1993) at the distance of each stellar group (Hernández et al. 2005); dashed lines represent the 10 Myr and 5 Myr isochrones (Palla & Stahler 1993) for OB1a and OB1b, respectively. Dot-dashed lines (for the ZAMS) and dotted lines (for the isochrones) show the region expected when the extinctions and the errors of the distances are included in the evolutionary models. Stars above these regions are foreground objects (X's), so we rejected them as members of OB1a and OB1b. Since the motion of the Ori OB1 association is mostly directed radially away from the Sun, the expected intrinsic proper motions in right ascension and declination are small. Using the proper motions in Kharchenko (2001), we rejected 7 stars in OB1a and 14 stars in OB1b, with a relative large intrinsic proper motions, applying the criterion defined by Brown et al. (1999). For the leftover objects (likely members), 93% of the stars in OB1a and 62% of the stars in OB1b have MIPS detections; most stars without [24] measurements (open square) exhibit 2MASS photometry characteristic of stars later than F0. Comparing 2MASS sources with and without MIPS detections in each stellar group, we find that the samples are complete for stars with $J \leq 10$. Using the distances, ages and reddening in Table 1 we estimate that this completeness limit corresponds roughly to a F0 stars in OB1a and to a A8 star in OB1b. However, since we detect stars with and without $24\mu\text{m}$ excess in our faintest limits (F5), the selected stars are representative samples of intermediate mass stars in both fields. Our final samples of early type stars include 26 objects in OB1a field and 34 objects in Orion OB1b field.

We find that 28 of the stars in our sample show excesses at $24\mu\text{m}$ above the photospheric colors (§3); optical spectra were obtained for these stars using the 1.5 m telescope of Whipple Observatory with the FAST Spectrograph (Fabricant et al. 1998), equipped with the Loral 512 x 2688 CCD. The spectrograph was set up in the FAST standard configuration (3400Å of spectral coverage centered at 5500Å, with a resolution of $\sim 6\text{\AA}$). These data set were used for spectral classification following the methods described in Hernández et al. (2004) and for discriminating stars with and without emission lines. In Figure 3 we show FAST spectra for the three emission line stars in our sample: the classical Be (CBe) star 25 Ori (Yudin 2001; Hernández et al. 2005; Briceño et al. 2006), and the two HAeBe stars (V346 Ori and HD290543). We also show the spectrum for the star HD36444 which does not exhibit emission lines and has a large $24\mu\text{m}$ excess (see §3).

Table 2 shows spectroscopic & photometric data for the intermediate and high mass

members found in OB1a and OB1b. Columns 1 and 2 show the 2MASS denomination and other names of the stars. Columns 3, 4, 5 and 6 show the IRAC magnitudes for the sample. The typical errors in these values are dominated by the uncertainties in the zero points magnitudes, 0.02-0.05 mag (Hartmann 2005). Columns 7 and 8 show [24] MIPS data in magnitudes and fluxes, respectively. The typical errors in MIPS photometry are 0.03-0.06 mag. Column 9 shows the excess ratio of the measured flux at 24 μm to that expected from the stellar photosphere (see next section). Spectral types and their references are shown in columns 10 and 11. The last column shows the disk type around each star (see next section).

3. Results

3.1. Observational analysis

Figure 4 shows the color-color diagram, [J-H] versus K-[24], for the early type stars selected as described in §2. Arrows represent the reddening vector for $A_V=1$. There are clearly three regions in the diagrams. The first one is the main sequence region, which is defined using the K-[24] distribution of the stellar sources compiled by Kharchenko (2001) on the low reddening region OB1a. This distribution describes a Gaussian centered at K-[24]=0.02 with $\sigma=0.10$ mag, and represents the 3σ boundaries on non-excess stars at 24 μm (dotted lines). The second one is the region located between the main sequence region and the color of the star HR4796A (K-[24]~5.0; dashed lines), which is the star with the largest 24 μm excess in the data set of debris disk objects compiled by Rieke et al. (2005); stars with optically thin disks like Vega type stars are located in this region (Gorlova et al. 2004; Young et al. 2004, ; hereafter debris disk region). The CBe star 25 Ori (filled square) in OB1a, with small NIR excess (upper-left panel in Figure 2) and with $\text{H}\alpha$ in emission (Figure 3), is also located in this region. In this case the 24 μm excess originates in a gaseous envelope, in which the emission lines and the NIR continuum excess are produced by free-free emission process. The third region is where stars with strong infrared excesses due to optically thick disks, that is the HAeBe stars, are located. The well known HAeBe star V346 Ori (Figure 3; Hernández et al. 2005; Vieira et al. 2003; The et al. 1994) appears in this last region (filled triangle).

The lower panel in Figure 4 reveals that the stars in the debris disk region in OB1b have systematically less 24 μm excess in comparison with OB1a; only two stars in OB1b, HD290543 and HD36444 (see below), have relative strong 24 μm excess. The larger 24 μm excess in OB1a is confirmed by Figure 5, which shows a comparison of the distributions of the K-[24] colors (left panels) and the spectral types (right panels) for the stars in the debris disk region in the OB1a (upper panels) and OB1b (lower panels) fields. We do not include in this

plot the CBe star 25 Ori. The difference in the K-[24] histograms between OB1a and OB1b is confirmed by a Kolmogorov-Smirnov (KS) test showing a significance level is only 5%. In contrast to the K-[24] distributions, the spectral type distributions for both regions are very similar, with a significance level of 75% in a KS test indicating that we are comparing similar populations. Also the fraction of debris disk stars candidates in OB1b ($\sim 38 \pm 3\%$) appears to be slightly lower than in OB1a ($\sim 46 \pm 4\%$). This indicates that the debris disk phenomenon appears to be more frequent and stronger in the older sub-association, OB1a.

Figure 6 shows the color-color diagrams, [5.8]-[8.0] versus [3.6]-[4.5] (upper panels) and [4.5]-[8.0] versus K-[4.5] (lower panels), for OB1a (left panels) and for OB1b (right panels). The errors bars for the stars 25 Ori, V346 Ori, HD290543 and HD36444 include the uncertainties from saturation effect, which were estimated using the deviation from the expected photospheric colors for the brightest objects detected in each IRAC band. Most of the stars in both sub-associations have photospheric IRAC colors. The HAeBe star V346 Ori has strong excess in the IRAC bands originated in its primordial disk. The CBe star appears to have excess in the color [4.5]-[8.0]; the error bars in the others colors reach the photospheric regions, so it is not possible estimated excess in those colors. The nature of the stars HD290543 and HD36444 in OB1b is reported for first time in this work:

- The star HD290543 (triangle) is located in the HAeBe loci on the NIR color color diagram (upper-right panel in Figure 2), shows H α emission in its spectrum (Figure 3), and exhibits large excess at $24\mu\text{m}$ (Figure 4) and in the IRAC bands (Figure 6), confirming it as a new HAeBe in the OB1b sub-association. Upper panel in Figure 7 shows the spectral energy distribution (SED) of HD290543. For comparison, the SEDs of the star V346 Ori (symbol X), and the photosphere (solid line; Kenyon & Hartmann 1995) of a star with a similar spectral type (A7) are displayed.

- The star HD36444 does not exhibit NIR excess in Figure 2 and have spectral type B9 without emission lines in its spectrum (Figure 3). This star is the only object located in the debris disk region in Figure 4 that shows excess in [8.0] IRAC band² (Figure 6). The lower panel of Figure 7 shows the SED for HD36444, for comparison, the SEDs of the star HR4796A (dotted line; Wahhaj et al. 2005), which defines the debris disk region in Figure 4, the SED of the star β Pic (dashed line); data from Hipparcos, 2MASS, IRAS catalogs and Telesco et al. (2005), and the photosphere for A0 type star (solid line; Kenyon & Hartmann 1995) are displayed. This comparison indicates that the SED of HD36444 is similar to that of β Pic, suggesting that these objects have similar evolutionary stages.

²HD36444 is out of the IRAC fields at [3.6] and [5.8]

3.2. Debris disk evolution

Figure 8 shows the excess emission at $24\mu\text{m}$, calculated as the ratio of the observed flux to that expected from the stellar photosphere, for intermediate mass stars in several stellar groups spanning a range of age from ~ 2.5 Myr to ~ 150 Myr. We use the color $K-[24]$ to determine this excess ratio (E_{ratio}). At these long wavelength, the photospheric colors are null and independent of spectral types (Figure 4; see also Gorlova et al. 2004; Young et al. 2004; Rieke et al. 2005). So, for Orion OB1a and Orion OB1b sub associations (open circles), $E_{ratio}=10^{(K-[24]-0.02)/2.5}$, where 0.02 is the mean value of $K-[24]$ (see §3.1). Our definition of stars with excess (see Figure 4) agrees with that given by Rieke et al. (2005), which is represented as a solid horizontal line ($E_{ratio}=1.25$). Other stellar groups included in Figure 8 are: IC 348 (Lada et al. 2006) with age of 2-3 Myr (star symbol), NGC2547 (Young et al. 2004; Rieke et al. 2005) with age of 25 Myr (open triangles), M47 (Gorlova et al. 2004; Rieke et al. 2005) with age of 100 Myr (open square) and NGC2516 (Rieke et al. 2005) with age 150 Myr (inverse open triangle). Similarly to our objects in Orion, these stellar groups are within 500 pc from the sun and have been observed using the MIPS scan mode to mapping large regions, so together they provide an excellent data set for statistical proposes. In addition, they have more reliable stellar ages than individual objects in the sky. The dashed line represents the median value of E_{ratio} for the stars with excess at $24\mu\text{m}$ in those stellar groups. By comparison, we include also stars observed by Rieke et al. (2005) using the MIPS point source mode or compiled for them from IRAS data (symbol X). Some stars with $E_{ratio}>8$ (hereafter, massive debris disks) are represented by arrows: from left to right, HD36444 (5 Myr) with $E_{ratio}=11.8$, HR4796A (8 Myr) with $E_{ratio}=97.2$, β Pic (20 Myr) with $E_{ratio}=21.9$, and HD21362 (80 Myr) with $E_{ratio}=8.4$. These observations have been compared with the results of two collisional cascade models for A type stars (Kenyon & Bromley 2004b, 2005, hereafter KB models): an “outer model” for the region from 30 AU to 150 AU (dot-dashed line), where the icy planets are formed, and an “inner model” for the region from 3 AU to 20 AU (dotted line), where rocky planets are expected to grow.

The outer KB model predicts that icy objects ($\sim 1000\text{-}3000$ Km) begin to form at the inner edge of the model at $\sim 10\text{-}20$ Myr. These objects stir up leftover planetesimals along their orbits and initiate a collisional cascade, in which smaller planetesimals ($\sim 1\text{-}10$ Km) are slowly ground into the fine dust observed in debris disks around young stars. The luminosity of the debris disk declines exponentially with stellar age, since the reservoir of smaller objects diminishes and the products from the collisions are removed mainly by radiation pressure and Poynting-Robertson drag (e.g., Dominik & Decin 2003; Chen et al. 2006). Since the KB models do not include the sublimation of ices, the excesses observed in the inner model could be overestimated. In particular, grains of water ice (H_2O) begin to sublimate at ~ 120 K (Fraser et al. 2001); assuming that the dust particles act like a black body in radiative

equilibrium (Chen et al. 2006), for an A0 star ($T_{\text{eff}}=9760$ K, $R=2.4$ R_{\odot}) this temperature is reached at ~ 37 AU from the star; the sublimation is completed at 18 AU where the grain temperature is ~ 170 K. The central clearing observed in some debris disks can be explained if the ice sublimation is an important mechanism for dust removal (Chen et al. 2006; Decin et al. 2003). The KB models have been scaled (scale factor ~ 0.5) and shifted (~ 0.3 in log time units) in Figure 8, so the peak in the outer model agrees with the peak observed in debris disk at 10 Myr (Orion OB1a). The vertical scale factor can be explained if: a) the dust production per collision is less than the model’s prediction (e.g., interactions between solid bodies and the gas damp particle velocities and remove particles from the model grid); or/and b) icy sublimation diminishes the dust produced at 30-37 AU from the star. Since the initial conditions in the KB models include objects with radius ~ 1 -1000 m (Kenyon & Bromley 2004b), the zero point for the age in the KB models could be different to that from the stellar evolution studies (e.g., Palla & Stahler 1993). However, since the growth time to reach objects with diameters of a few meters in the disk is relatively short ($\lesssim 10^6$ yr; Weidenschilling 1997; Dullemond & Dominik 2005), this zero point difference is not significant for stars with few Myr or older (Kenyon 2006, private communication). Besides the zero point differences in age, the shift in the age of the KB models could be explained if: a) the timescales from KB models are $\sim 30\%$ to $\sim 40\%$ longer than the actual evolution times, due the radial resolution in the grids (Kenyon & Bromley 2004b); and/or b) cascade collisions occur in the region between the inner and outer model (20-30AU), where the 1000 Km objects could be formed faster than in the outer model (see Kenyon & Bromley 2002, 2004b, 2005, for more details about uncertainties and limits of the models).

In general terms, observations of debris disks follow the trend predicted by the KB models. The upper envelope in excess ratio in debris disks with age $\gtrsim 10$ Myr can be fitted by the KB outer model. In Orion OB1b, at 5 Myr old, the outer KB model does not predict enough excess emission to explain the observed excesses. A small dust contribution from collisional cascade in the inner disk ($\lesssim 20$ -30AU) or remaining primordial dust in the disk could explain the differences. In IC 348 (~ 2.5 Myr) statistical fluctuations due to the small size of the sample could be important; on the other hand, the relative large excess could be explained if there was a significant amount of remaining primordial dust in the disk, and these objects were in an intermediate phase between HAeBe and debris disks.

The stars with massive debris disks could be explained if the observed dust is produced by eventual collisions between 2 large objects ($\gtrsim 1000$ Km; Kenyon & Bromley 2004b, 2005). However, an alternative explanation for younger stars ($\lesssim 20$ Myr) is that those objects are in a phase between HAeBe star and true debris systems (Rieke et al. 2005) retaining some of the primordial dust. In any case, our observations confirm that this intermediate phase has to be very brief; if the star HD36444 is in this phase, the fraction at 5 Myr (OB1b) is

~3%, and null if the $24\mu\text{m}$ excess in HD36444 is from a massive debris disk. In contrast to the small fraction of primordial disk reported in Hernández et al. (2005) for the association OB1 (3-5%), the total disk fractions (primordial disks + debris disks) are 50% and 40% for OB1a and OB1b, respectively. Since some objects could have a cooler disks, which are not detected at $24\mu\text{m}$, these fractions are inferior limits. So, most of the stars in the mass range of HAeBe are born surrounded by disks, which evolve to debris disks in few Myr.

4. Conclusions

We have combined Spitzer IRAC and MIPS observations, 2MASS data, and optical spectra to study the properties of the disks around early type stars (B, A, F) in fields of two sub-associations of Orion OB1: OB1a with an age of 10 Myr (Briceño et al. 2006) and OB1b with an age of 5 Myr (Briceño et al. 2005). In each field we find only one star with an optically thick disk which identifies them as a HAeBe star; of these, V346 Ori in Ori OB1a was already known (e.g., Hernández et al. 2005; Vieira et al. 2003; The et al. 1994), but HD290543 in Ori OB1b is reported here for the first time. The star HD36444 in OB1b is the only non-emission line star in our sample with excess at the IRAC [8.0] and the MIPS [24] bands. The SED of this object is similar to that of β Pic; both objects have a relatively large $24\mu\text{m}$ excess that could be explained if they have massive debris disks produced by the eventual collisions between two large ($>1000\text{ Km}$) objects (Kenyon & Bromley 2005, 2004b). An alternative explanation could be that these objects are in a intermediate phase between HAeBe and true debris systems (Rieke et al. 2005). The small or null fraction of objects in this phase found in our samples confirms that the lifetime of this intermediate phase is very brief.

We find a population of early type stars without excess in the IRAC bands and without emission lines in their optical spectra, but with varying degrees of K-[24] excess. We identify these stars as debris disks. We find that in the older OB1a sub-association, the debris disk phenomenon, diagnosed by the mid-IR excess, is stronger and more frequent than in the younger sub-association OB1b.

We have put together our observations with those of other stellar groups of different ages, and compared them with the theoretical models of Kenyon & Bromley (2005). We find a peak in the debris disk phenomenon at 10 Myr indicated by our observations of Ori OB1a in agreement with theoretical predictions, in which the peak is associated to the formation of large icy objects (1000 Km) in 10-20 Myr, which stir up the smaller objects in the disk and produce a collisional cascade, in which $\sim 1-10\text{ Km}$ planetesimals are converter in fine dust grains (Kenyon & Bromley 2004b, 2005). Stellar groups older that 10 Myr follow the

predictions of collisional cascades in the outer model (30-150 AU, where the icy planets are formed) proposed by Kenyon & Bromley (2005) for A type star. The relative small excess and small fraction of debris disks observed at 5 Myr (Ori OB1b) could be associated to a phase between the clearing of the primordial disk, <3Myr (Hernández et al. 2005), and the formation of large icy objects, 10-20Myr (Kenyon & Bromley 2004b). In this phase, small amount of remaining primordial dust and small production of second generation dust are expected. On the other hand, these amounts of dust (remaining primordial dust and/or second generation dust) could explain the differences between our observations at 5 Myr (OB1b) and the outer model of Kenyon & Bromley (2005). The large excesses in the younger stellar group IC 348 (\sim 2.5 Myr) could indicate that a significant amount of primordial dust remains in the disk. However, small statistical number fluctuation can affect the excesses observed and a more detailed study is necessary to establish the presence of primordial dust in these systems.

5. Acknowledgments

We thank Scott Kenyon for useful comments and for providing us the models plotted in Figure 8, Francesco Palla for providing the isochrones of PMS stars, and Massimo Marengo for insightful communications. We also thank Perry Berlind and Susan Torkarz of the SAO Telescope Data Center for carrying out the observation and data reduction of the spectra. This publication make use of data products from the Two Micron All Sky Survey, which is a joint project of the University of Massachusetts and the Infrared Processing and Analysis Center/California Institute of Technology. This work is based on observations made with the Spitzer Space Telescope (GO-1 3437), which is operated by the Jet Propulsion Laboratory, California Institute of Technology under a contract with NASA. Support for this work was provided by NASA through an award issued by JPL/Caltech. This publication was supported in part by the NASA grants NAG5-9670 and NAG10545, NSF grant AST-9987367 and grant No. S1-2001001144 of FONACIT, Venezuela.

REFERENCES

Bessell, M. S. & Brett, J. M. 1988, PASP, 100, 1134

Briceño, C., Hartmann, L., Hernández, J., Calvet N., Vivas, A. K., Furesz G., Szentgyorgyi A. 2005, submitted to ApJ

Briceño, C., Calvet, N., Hernández, J., Vivas, A. K., Hartmann, L., Downes, J. J., & Berlind, P. 2005, AJ, 129, 907.

Bryden, G., et al. 2006, ApJ, 636, 1098

Brown, A. G., Walter, F. M., & Blaauw, A. 1999, in ASP Conf. Ser., The Orion Complex Revisited, ed. M.J. McCaughrean & A. Burkert.

Calvet, N., et al. 2005, ApJ, 630, L185

Calvet, N., Muzerolle, J., Briceño, C., Hernández, J., Hartmann, L., Saucedo, J. L., & Gordon, K. D. 2004, AJ, 128, 1294

Calvet, N., D'Alessio, P., Hartmann, L., Wilner, D., Walsh, A., & Sitko, M. 2002, ApJ, 568, 1008

Cardelli, J. A., Clayton, G. C., & Mathis, J. S. 1989, ApJ, 345, 245

Cutri, R. M., et al. 2003, VizieR Online Data Catalog, 2246, 0

Chen, C. H., Jura, M., Gordon, K. D., & Blaylock, M. 2005a, ApJ, 623, 493

Chen, C. H., et al. 2005b, ApJ, 634, 1372

Chen, C. H., et al. 2006, ArXiv Astrophysics e-prints, arXiv:astro-ph/0605277

Cox, A. N. 2000, Allen's astrophysical quantities, 4th ed. Publisher: New York: AIP Press; Springer, 2000. Edited by Arthur N. Cox. ISBN: 0387987460.

D'Alessio, P., et al. 2005, ApJ, 621, 461

Decin, G., Dominik, C., Waters, L. B. F. M., & Waelkens, C. 2003, ApJ, 598, 636

Dominik, C., & Decin, G. 2003, ApJ, 598, 626

Dullemond, C. P. & Dominik, C. 2004, A&A, 417, 159

Dullemond, C. P., & Dominik, C. 2005, A&A, 434, 971

ESA. 1997, The Hipparcos and Tycho Catalogues (ESA SP-1200) (Noordwijk: ESA)

Fabricant, D., Cheimets, P., Caldwell, N., & Geary, J. 1998, PASP, 110, 79

Fazio, G. G., et al., 2004, ApJS, 154, 10

Fraser, H. J., Collings, M. P., McCoustra, M. R. S., & Williams, D. A. 2001, MNRAS, 327, 1165

Gordon, K. D., et al. 2005, PASP, 117, 503

Gorlova, N., et al. 2004, ApJS, 154, 448

Haisch, K. E., Lada, E. A., & Lada, C. J. 2001, ApJ, 553, L153

Hartmann, L. 2005, ASP Conf. Ser. 337: The Nature and Evolution of Disks Around Hot Stars, 337, 3

Hernández, J., Calvet, N., Briceño, C., Hartmann, L., & Berlind, P. 2004, AJ, 127, 1682

Hernández, J., Calvet, N., Hartmann, L., Briceño, C., Sicilia-Aguilar, A., & Berlind, P. 2005, AJ, 129, 856.

Hillenbrand, L., Carpenter, J., & Meyer, M. 2005, AJ, in preparation.

Kenyon, S. J. & Bromley, B. 2002, AJ, 123, 1757

Kenyon, S. J. & Bromley, B. 2004a, ApJ, 602, 136

Kenyon, S. J. & Bromley, B. 2004b, AJ, 127, 513

Kenyon, S. J. & Bromley, B. 2005, AJ, 130, 269

Kenyon, S. J. & Hartmann, L. 1995, ApJS, 101, 117

Kharchenko, N. V. 2001, Kinematika i Fizika Nebesnykh Tel, 17, 409.

Lada, E. A., & Lada, C. J. 1995, AJ, 109, 1682

Lada, C. J., et al. 2006, AJ, 131, 1574

Muzerolle, J., et al. 2006, in prep.

Muzerolle, J., D'Alessio, P., Calvet, N., & Hartmann, L. 2004, ApJ, 617, 406.

Muzerolle, J., Hillenbrand, L., Calvet, N., Briceño, C., & Hartmann, L. 2003, ApJ, 592, 266

Nesterov, V. V., Kuzmin, A. V., Ashimbaeva, N. T., Volchkov, A. A., Röser, S., & Bastian, U. 1995, A&AS, 110, 367

Palla, F. & Stahler, S. W. 1993, ApJ, 418, 414

Rieke, G. H., et al, 2004, *ApJS*, 154, 25

Rieke, G. H., et al. 2005, *ApJ*, 620, 1010

Schlegel, D. J., Finkbeiner, D. P., & Davis, M. 1998, *ApJ*, 500, 525

Schmidt, E. G., & Carruthers, G. R. 1993, *ApJS*, 89, 259

Schuster, M., Marengo, M., Patten, B. 2006, in Proceedings of the SPIE Meeting Astronomical Telescopes and Instrumentation 2006, Orlando, Florida, USA, May 24-31, 2006.

Sicilia-Aguilar, A., Hartmann, L. W., Hernández, J., Briceño, C., & Calvet, N. 2005, *AJ*, 130, 188

Sicilia-Aguilar, A., et al. 2006, *ApJ*, 638, 897

Telesco, C. M., et al. 2005, *Nature*, 433, 133

The, P. S., de Winter, D., & Perez, M. R. 1994, *A&AS*, 104, 315

Vieira, S. L. A., Corradi, W. J. B., Alencar, S. H. P., Mendes, L. T. S., Torres, C. A. O., Quast, G. R., Guimarães, M. M., & da Silva, L. 2003, *AJ*, 126, 2971

Weidenschilling, S. J. 1997, *Icarus*, 127, 290

Wahhaj, Z., Koerner, D. W., Backman, D. E., Werner, M. W., Serabyn, E., Ressler, M. E., & Lis, D. C. 2005, *ApJ*, 618, 385

Young, E. T., Lada, C. J., Teixeira, P., Muzerolle, J., Muench, A., Stauffer, J., Beichman, C. A., Rieke, G.H., Hines,D.C., Su, K. Y., Engelbracht, C.W., Gordon, K.D., Misselt, K, Morrison, J. Stansberry J., and Kelly D. 2003, *AJ*, 126, 2971

Yudin, R. V. 2001, *A&A*, 368, 912

Table 1. MIPS fields

Name	D_{Ref} pc	Age Myr	α_C Deg	δ_C Deg	Area Deg ²	$A_V(\text{ref})$ mag ¹
Ori OB1a	335±13	10	81.2986	1.6438	1.10	0.12
Ori OB1b	443±18	5	82.7585	-1.7050	1.42	0.60

¹90% of the field have $A_V < A_V(\text{ref})$

[–]Distances from Hernández et al. (2005)

[–]Ages from Briceño et al. (2005, 2006)

Table 2. Intermediate mass stars in OB1a and OB1b

2MASS	Name	[3.6] mag	[4.5] mag	[5.8] mag	[8.0] mag	[24] mag	$F_{24\mu\text{m}}$ mJy	Excess ratio	Spectral type	ref	Disk
Orion OB1a											
05224795+0143002	HD35150	9.43	9.41	9.37	9.24	7.64	6.39	5.61	A0	1	debris
05230192+0141489	HD35177	s	s	8.37	8.36	8.40	3.18	0.99	B8	2	no-disk
05230686+0118237	HD287787	9.96	...	9.59	...	8.66	2.50	3.41	A7	1	debris
05231014+0108225	HD35203	8.25	3.67	0.91	B7	2	no-disk
05234591+0150334	HD287773	9.48	9.50	9.51	9.47	9.63	1.02	0.94	A2	4	no-disk
05235020+0132529	HD287845	9.46	9.46	9.40	9.38	9.39	1.28	1.14	F5	4	no-disk
05240786+0138000	HD35332	9.38	9.36	9.32	9.24	7.24	9.32	7.30	B9	1	debris
05241272+0134121	HD287846	9.82	9.88	9.79	9.81	7.79	5.58	6.79	F4	1	debris
05241300+0146421	HD35351	9.16	9.09	9.10	9.01	8.24	3.68	2.11	A0	1	debris
05241392+0115432	HD287860	8.24	3.68	2.76	F6	1	debris
05241447+0151479	...	9.86	9.89	9.84	9.83	9.99	0.74	0.96	no-disk
05242074+0135266	HD35367	9.58	9.57	9.58	9.52	8.03	4.47	4.30	A1	1	debris
05242421+0141333	HD287842	9.35	9.34	9.36	9.31	9.37	1.30	1.06	A3	4	no-disk
05243861+0148388	HD35409	s	s	8.44	8.43	8.29	3.53	1.18	A	3	no-disk
05244482+0150472	25 Ori	s	s	s	s	3.52	284.12	5.40	B1	1	CBe
05245456+0158083	HD287838	...	9.35	...	9.25	9.44	1.22	0.96	A2	4	no-disk
05251029+0115314	HD287861	7.47	7.48	7.09	A3	1	debris
05251139+0155242	HD35501	s	s	7.62	7.61	7.78	5.64	0.83	B8	2	no-disk
05251164+0133296	HD287847	9.52	9.51	9.47	9.46	9.47	1.19	1.12	A3	4	no-disk
05253978+0138183	HD287850	9.67	9.64	9.50	9.59	8.93	1.95	2.12	A9	1	debris
05254865+0123220	HD287854	9.73	...	9.68	...	8.16	3.99	4.48	F0	1	debris
05260368+0148293	HD287851	9.83	9.83	9.79	9.75	8.87	2.07	2.56	F3	1	debris
05261198+0153357	HD35625	9.33	9.28	9.25	9.24	8.32	3.42	2.50	A0	1	debris
05264810+0204058	HD35716	s	8.68	...	8.66	8.83	2.14	0.85	B9	2	no-disk
05271919+0136224	HD35791	9.00	8.90	8.91	8.89	8.95	1.92	0.99	B9	5	no-disk
05244279+0143482	V346 Ori	s	s	6.12	5.36	2.12	1034.41	376.36	A9	1	primordial
Orion OB1b											
05285515-0145387	HD36057	8.28	3.57	1.09	A0	3	no-disk
05291353-0147463	HD290534	9.48	9.46	9.46	9.40	8.38	3.25	2.73	F2	1	debris
05291785-0143391	HD290533	9.53	9.54	9.49	9.48	9.64	1.01	0.92	F8	4	no-disk
05292120-0200309	HD36118	s	s	8.54	8.58	8.73	2.34	0.94	A0	3	no-disk
05292269-0131537	HD290530	9.37	9.28	...	9.16	8.97	1.89	1.48	F8	1	debris
05292958-0215399	HD294152	8.70	2.43	2.49	F4	1	debris
05294888-0139281	HD36176	s	s	8.78	8.63	8.86	2.09	0.93	A0	3	no-disk
05295026-0102088	HD290521	8.78	2.24	1.80	A6	1	debris
05295547-0215163	HD36185	s	...	8.70	...	8.67	2.48	1.01	A0	3	no-disk
05300287-0208595	HD290548	10.02	...	9.94	...	9.48	1.18	1.74	F6	1	debris
05300439-0144584	HD36219	s	s	7.80	7.78	7.91	4.99	0.91	B8	2	no-disk
05301868-0201575	HD290543	s	s	6.42	5.16	2.13	1027.77	537.53	A7	1	primordial
05303822-0139029	HD290536	9.54	9.53	9.51	9.49	9.64	1.02	0.99	F2	4	no-disk

Table 2—Continued

2MASS	Name	[3.6] mag	[4.5] mag	[5.8] mag	[8.0] mag	[24] mag	$F_{24\mu\text{m}}$ mJy	Excess ratio	Spectral type	ref	Disk
05305984-0202024	HD290541	9.53	9.53	9.54	9.68	9.78	0.89	0.80	F0	4	no-disk
05312070-0158522	HD36393	s	s	8.68	8.61	8.48	2.96	1.19	B8	3	no-disk
05312120-0205569	HD36394	s	s	7.96	7.96	7.93	4.90	1.60	B9	1	debris
05313136-0149332	HD290540	9.50	9.51	9.47	9.39	8.75	2.31	2.02	A0	1	debris
05314048-0107332	HD36444	...	8.98	...	8.33	6.31	21.93	11.80	B9	1	debris ^a
05314469-0130582	...	9.92	9.87	...	9.80	9.14	1.61	2.11	F7	1	debris
05314814-0124566	HD290594	9.69	9.67	9.64	9.61	9.75	0.92	0.95	F5	4	no-disk
05315101-0159448	...	9.80	9.80	9.77	9.81	9.78	0.90	1.11	no-disk
05320405-0128445	HD36502	9.22	9.23	9.13	9.15	9.18	1.55	0.96	B9	3	no-disk
05320525-0137136	HD290598	9.69	9.70	9.70	9.66	9.05	1.75	1.79	A0	1	debris
05321963-0124133	HD290592	9.33	9.41	9.28	9.26	9.44	1.23	0.92	G0	4	no-disk
05322179-0101191	HD290585	8.92	1.97	3.23	F1	1	debris
05324082-0148341	HD290610	9.58	9.67	9.57	9.53	9.55	1.10	1.21	A0	4	no-disk
05324134-0135305	HD36591	s	s	6.00	5.87	6.31	21.91	0.68	B1	2	no-disk
05324164-0202131	HD36592	9.02	8.91	8.91	8.87	8.60	2.66	1.30	B9	3	no-disk
05324975-0211494	HD36617	s	...	8.39	...	8.18	3.92	1.14	A0	2	no-disk
05325042-0136026	HD290599	9.60	9.59	9.60	9.41	9.93	0.78	0.74	A2	4	no-disk
05330558-0143155	HD290609	6.96	11.96	4.01	B9	1	debris
05330734-0143021	HD36646	6.83	13.49	0.97	B3	2	no-disk
05331305-0203129	9.97	0.75	1.58	F5	1	debris
05331540-0143124	HD290608	9.05	1.76	1.01	B8	3	no-disk

^aMassive debris disk

^sSaturated

Note. — Spectral type reference: 1 This work; 2 Hernández et al. (2005); 3 Kharchenko (2001); 4 Nesterov et al. (1995); 5 Schmidt & Carruthers (1993)

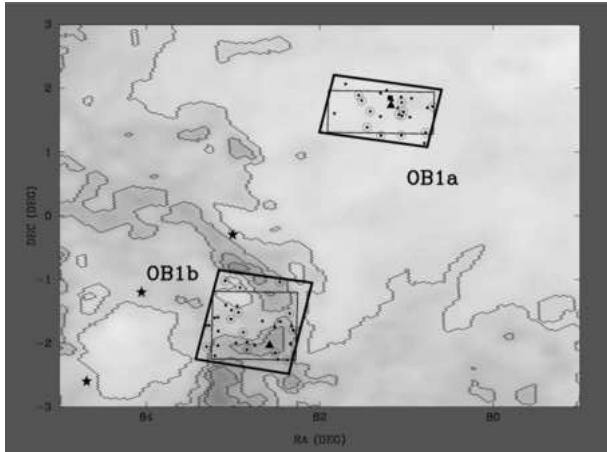


Fig. 1.— Observations in Orion OB1 association. The isocontours of the map of dust infrared emission (Schlegel et al. 1998) are indicators of galactic extinction ($A_V=0.2, 0.4, 0.6 \& 0.8$ mag). The Ori OB1b sub-association corresponds mostly to the belt region, and can be traced by the ringlike structure centering at $RA \sim 84$ and $DEC \sim -2$, whereas Ori OB1a spans the large low reddening area north and west of Ori OB1b. The thick boxes represent the MIPS fields and the thin boxes are the IRAC fields. Dots are the selected early type stars in each field. Open circles are objects with $24 \mu m$ excess (see §3). These stars, and stars indicated with a square (25 Ori in OB1a), and triangles (V346 Ori in OB1a and HD290543 in OB1b) have also been observed with the FAST spectrograph.

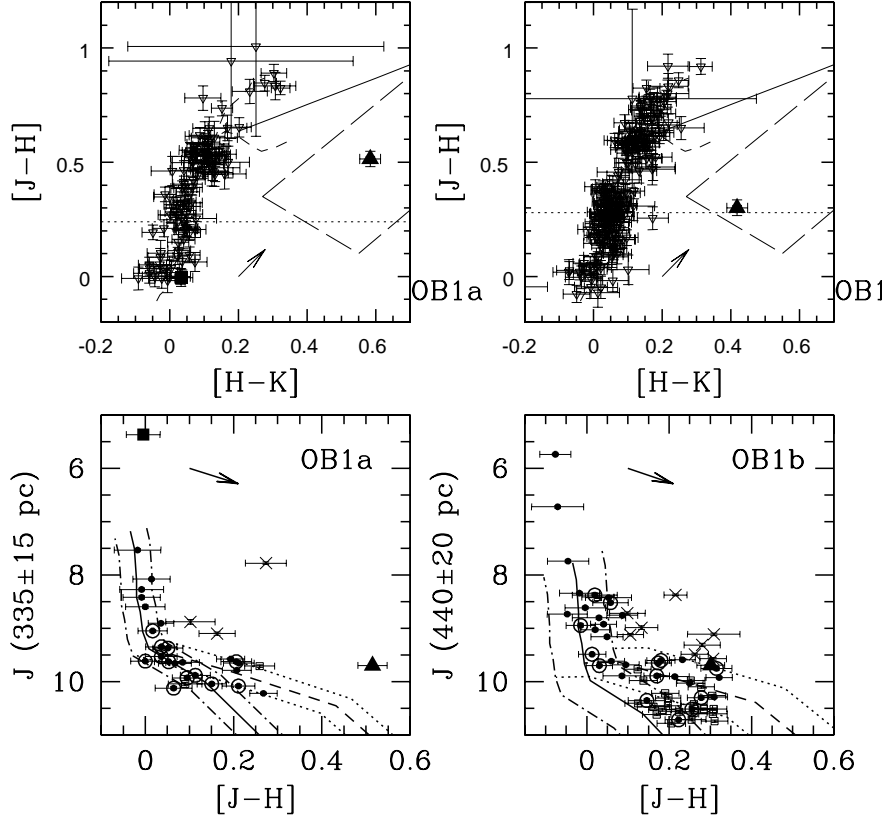


Fig. 2.— NIR color-color and color-magnitude diagrams illustrating the procedure for sample selection. The upper panels show the NIR color-color diagrams for stars with $J < 10.3$ for the OB1a field (left) and $J < 11.0$ for the OB1b field (right); the dotted lines represent the limits in $[J-H]$ color, 0.24 for OB1a and 0.28 for OB1b (see text). Most of the stars (inverse triangles), including the star 25 Ori (filled square), are located on the main sequence locus (dashed line; Bessell & Brett 1988). Only two objects (V346 Ori in OB1a and HD290543 in OB1b; filled triangles) appear in the HAeBe stars loci (long-dashed line; Hernández et al. 2005). By comparison the locus of low mass stars with primordial disks (CTTs) is indicated with a solid line. These HAeBe stars and the early type objects without NIR excess (below the $[J-H]$ limits) are plotted in the color-magnitude diagrams, J versus $[J-H]$ (lower panels). The solid lines and the dashed lines represent the ZAMS and the isochrones for the distance and the age of each stellar group. The dot-dashed lines (for the ZAMS) and the dotted lines (for the isochrones) show the regions expected when the extinctions and the errors of the distances (see Table 1) are included in the evolutionary models. Symbol X represents foreground objects located above these regions. Open squares are objects without MIPS detections. Filled circles represent stars selected in each sub-association, and the stars with $24\mu\text{m}$ excess are surrounded by open circles. Since 7 stars in OB1a and 14 stars in OB1b have large intrinsic proper motion, they are not included in the color-magnitude diagrams. Errors bars represent the uncertainties from 2MASS catalog, and the arrows are the reddening vectors for $A_V=1$.

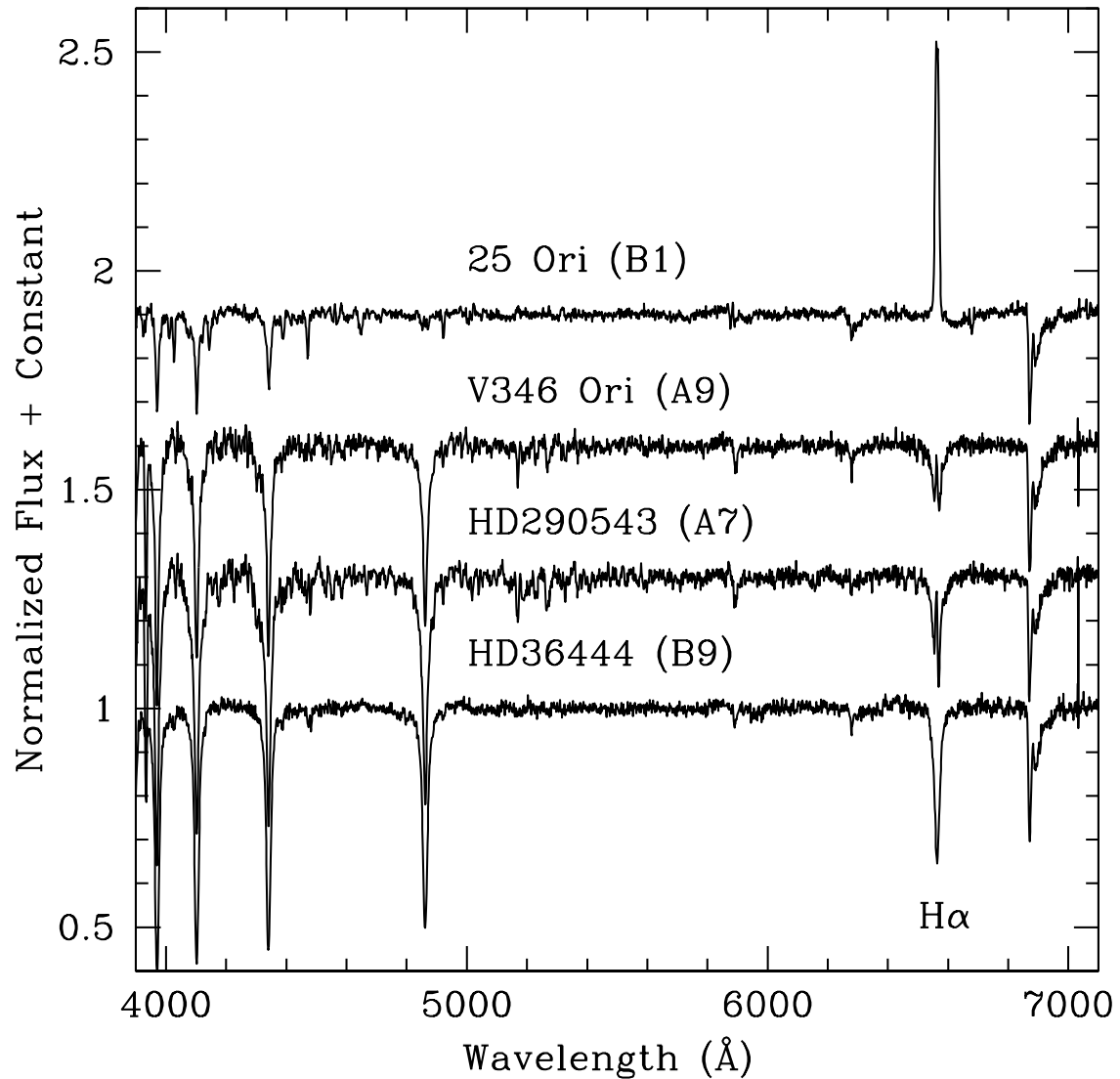


Fig. 3.— FAST spectra of 25 Ori, V346 Ori, HD290543, and HD36444. The three first spectra are the emission line stars (one CBe and two HAeBe) that we found in our data set. The last one is a star with large $24\mu\text{m}$ excess, which does not exhibit emission features in its spectrum.

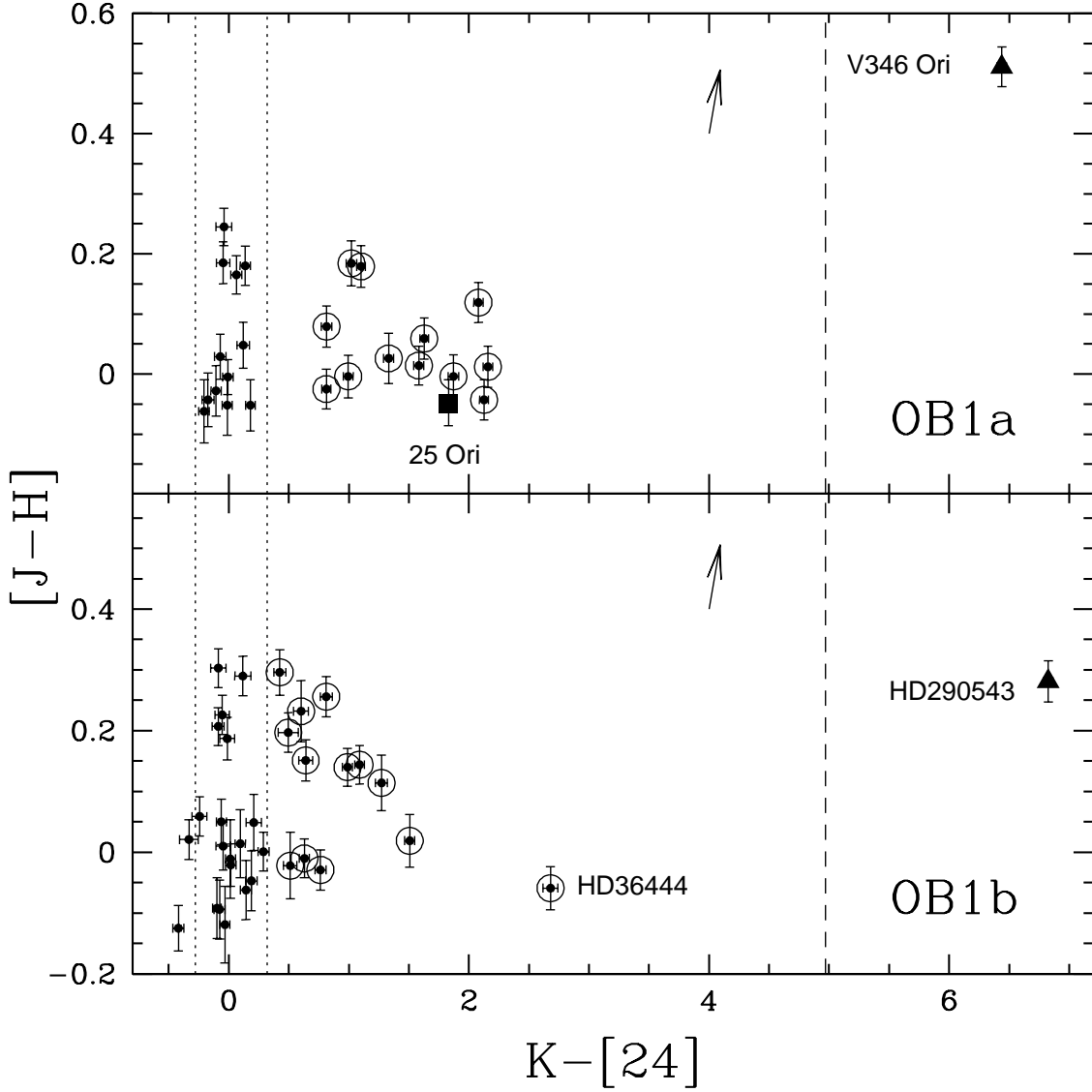


Fig. 4.— Location of the early type stars in the $[J-H]$ versus $K-[24]$ color-color diagrams. The upper panel corresponds to the OB1a field and the lower panel to the OB1b field. Symbols are the same as Figure 1. Arrows are the reddening vectors for $Av=1$. The dotted lines represent the main sequence limits defined using the 3σ boundaries ($\sigma=0.10$, $mean=0.02$) on the $K-[24]$ distribution of stellar sources compiled by Kharchenko (2001) for the low reddening OB1a field. The dashed line at $K-[24] \sim 5$ separates the debris disk/CBe region from the HAeBe region and corresponds to the color of the star HR4796A.

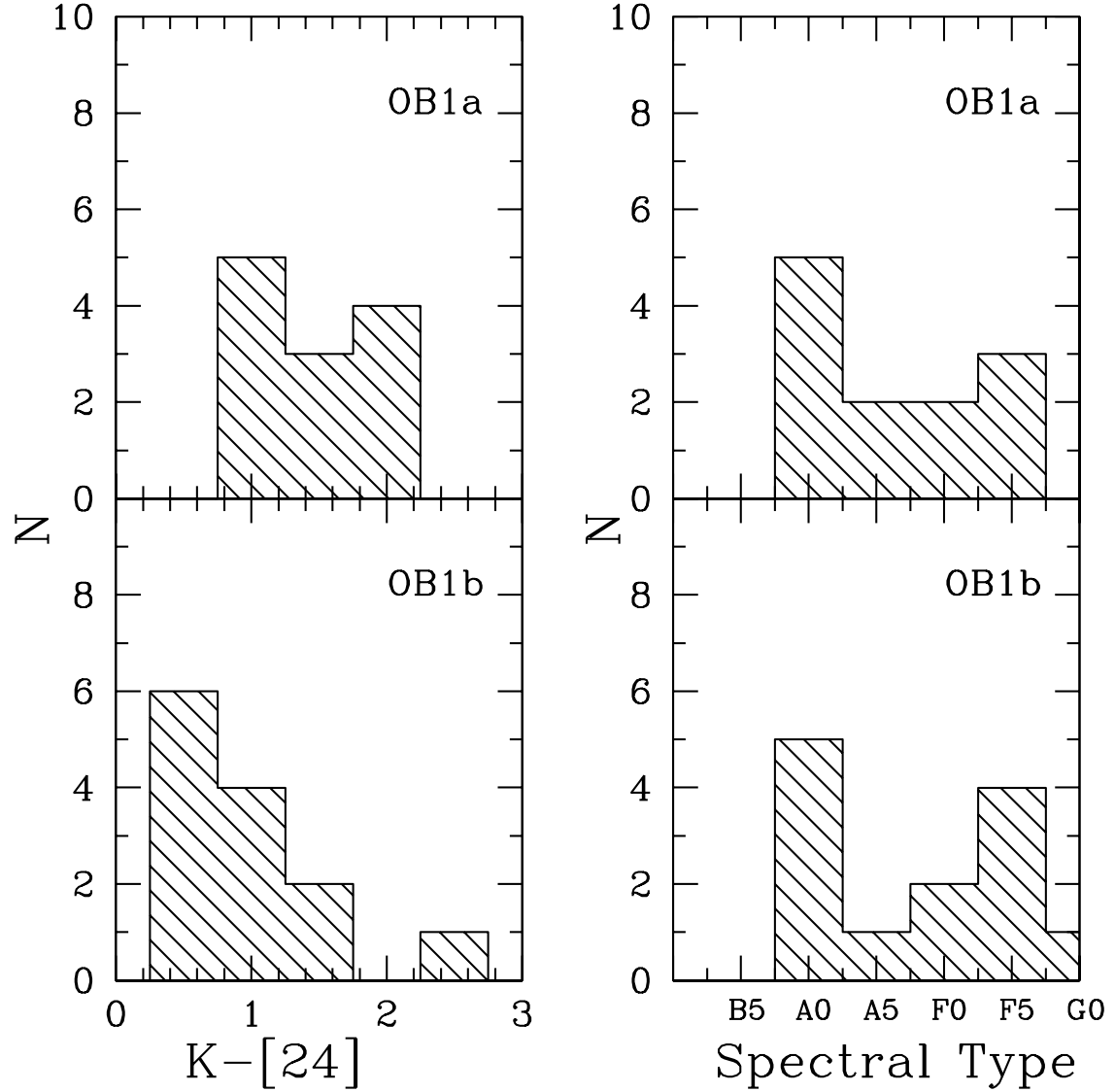


Fig. 5.— K-[24] (left panels) and spectral type (right panels) distributions for the 24 μ m excess stars in OB1a (upper panels) and OB1b (lower panels). We exclude the HAeBe stars (V346 Ori and HD290543) and the CBe star (25 Ori). A comparison of the distributions of spectral types shows a Kolmogorov-Smirnov significance level of 75%, indicating that we are comparing similar populations. In contrast, the K-[24] histogram on OB1b field appears displaced toward lower values of K-[24] excess than the OB1a field. A Kolmogorov-Smirnov test shows that the significance level in this case is 5%.

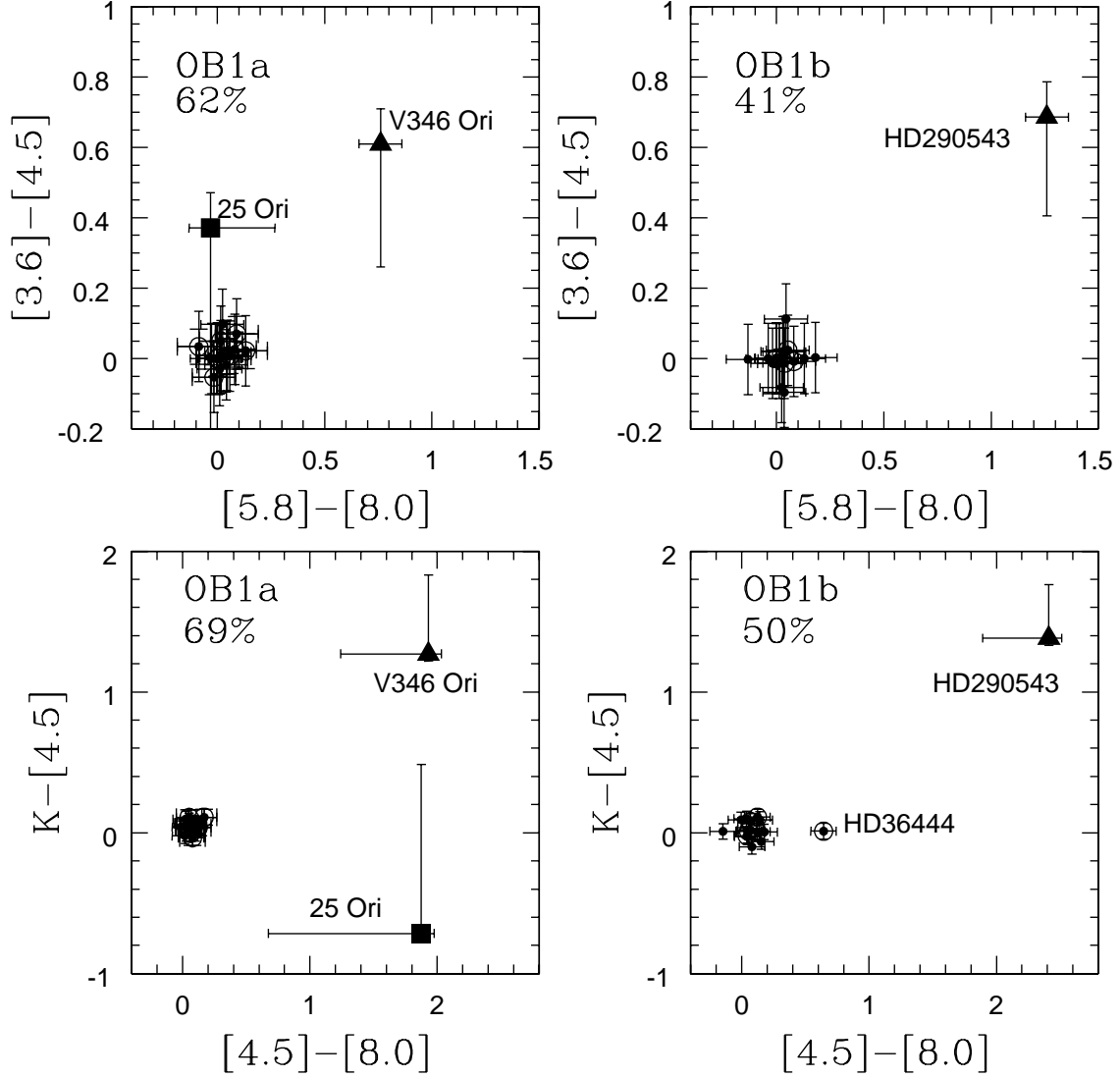


Fig. 6.— Color-color diagrams, $[5.8]-[8.0]$ versus $[3.6]-[4.5]$ (upper panels) and $[4.5]-[8.0]$ versus $K-[4.5]$ (lower panels). Symbols are the same as Figures 1 and 4. The error bars for the HAeBe stars and the CBe star include the uncertainties from saturation effect. The IRAC excesses on the HAeBe stars are apparent in these diagrams. The star HD36444 (not included in the upper panel) has excess at $8\mu\text{m}$, but not at $[4.5]$ IRAC band. The star 25 Ori appears to have small excess in $[4.5]-[8.0]$ color; since the error bars reach the photospheric region in the diagrams, excesses in other colors are not possible to estimate. We show the percent of the sample plotted in each panel.

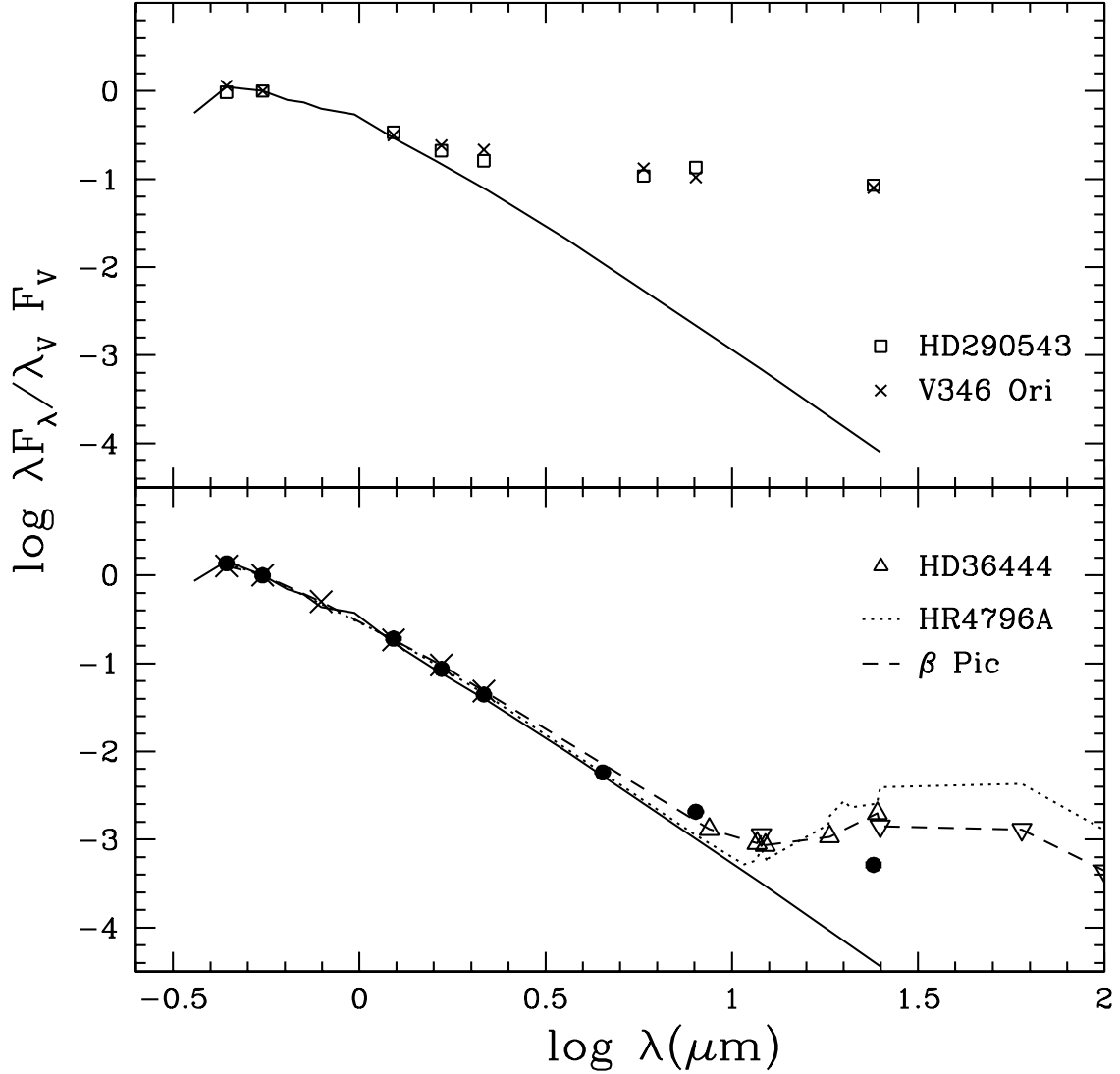


Fig. 7.— Spectral energy distributions of HD290543 and HD36444. The fluxes are calculated from the BV photometry (ESA 1997), 2MASS photometry (Cutri et al. 2003), and IRAC/MIPS magnitudes. In each case, fluxes have been corrected for reddening (estimated from the B-V color and the spectral type) using the standard reddening law, and have been normalized to the V band. In the upper panel, SEDs of the HAeBe stars, V346 Ori (symbol X, spectral type A8) and HD290543 (open squares) are displayed. For comparison, we also show the photospheric emission (solid line; Kenyon & Hartmann 1995) of a star with a similar spectral type of HD294503 (A7). The lower panel shows the SEDs of the star HD36444 (solid circles), the star HR4796A (dotted line; Wahhaj et al. 2005) and the star β Pic (dashed line). The SED of β Pic was derived from magnitudes in Hipparcos and 2MASS catalogs (X's), IRAS fluxes (inverse open triangles) and the mid-IR data from Telesco et al. (2005, open triangles) The solid line represents the photospheric emission of a star with spectral type B9.

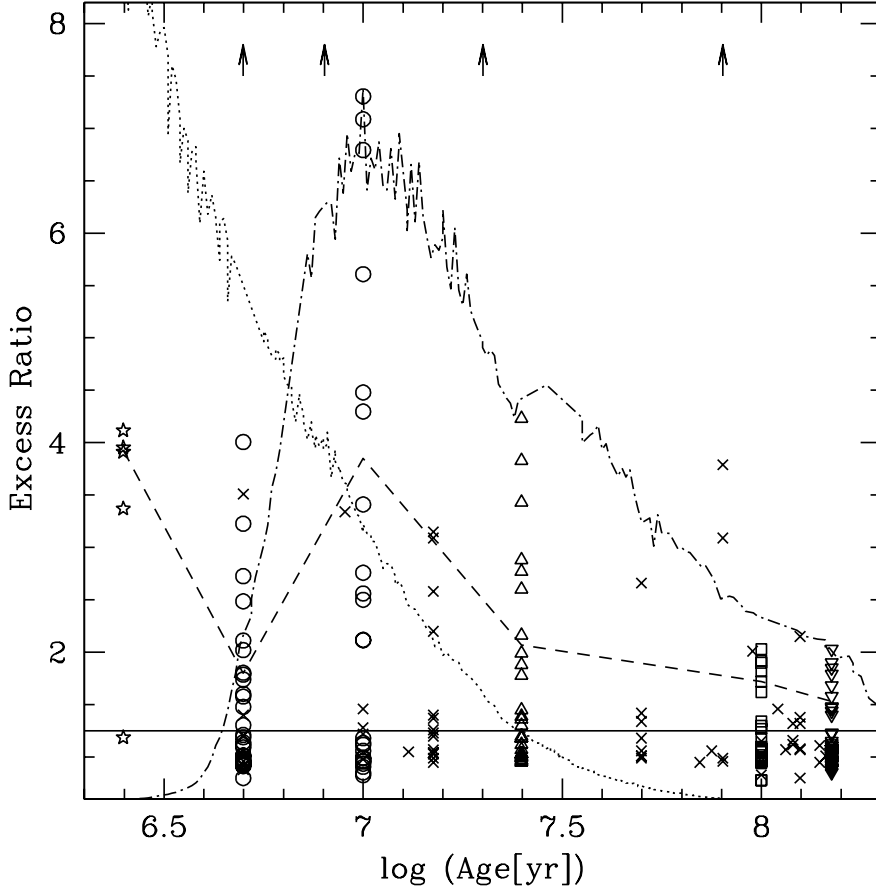


Fig. 8.— $24 \mu\text{m}$ excess versus logarithm of the age. The excess ratio is calculated as the ratio of the observed flux at $24 \mu\text{m}$ to that expected from the stellar photosphere. Our observations in OB1 association (open circles) are plotted with other stellar groups mapped with MIPS: IC 348 (star symbols, ~ 2.5 Myr; Lada et al. 2006), NGC2547 (Young et al. 2004; Rieke et al. 2005, open triangles, 25 Myr;), M47 (open square, 100 Myr; Gorlova et al. 2004; Rieke et al. 2005) and NGC2516 (inverse open triangles, 150Myr; Rieke et al. 2005). The solid line represents the definition of excess stars from Rieke et al. (2005), which agrees with our limit for debris disks (see Figure 4). The dashed line represents the median values for debris disk objects in each stellar group. The dotted line and the dot-dashed line represent the inner (3-20 AU) and the outer (30-150 AU) collisional cascade model from Kenyon & Bromley (2005), respectively. The stellar groups with age $\gtrsim 10$ follow the trend expected by the outer collisional cascade model. At 5 Myr collisional cascade in inner region (20-30 AU) or remain primordial dusts could explain the differences between the observation and the collisional cascade model at 30-150 AU. Since the models do not include ice sublimation process, the excess predicted by the inner model could be overestimated if the grains are icy in the inner region of the disk. In this case, a significant amount of primordial dust can be expected at IC 348. By comparison, we include stars observed by Rieke et al. (2005) using the MIPS point source mode or compiled for them from IRAS data (symbol X). The upward-pointing arrows are objects with a possible massive debris disks; from left to right, HD36444 (in Ori OB1b), HR 4796A, β Pic, and HD21362.